JARS Journal of Applied Remote Sensing

RESEARCH PAPER

Post-launch evaluation and improvements of National Oceanic and Atmospheric Administration-20 Visible-Infrared Imaging Radiometer Suite sensor data record geolocation accuracy

Slawomir Blonski,[a,*] **Wenhui Wang**,[b] **Khalil Ahmad**,[a] **and Changyong Cao**[c]
[a]Global Science and Technology, Inc., Greenbelt, Maryland, United States
[b]University of Maryland, CISESS/ESSIC, College Park, Maryland, United States
[c]NOAA/NESDIS/Center for Satellite Applications and Research, College Park, Maryland, United States

ABSTRACT. National Oceanic and Atmospheric Administration (NOAA)-20 (formerly Joint Polar Satellite System-1) is a polar-orbiting weather satellite launched on November 18, 2017. Visible-Infrared Imaging Radiometer Suite (VIIRS) is one of five instruments onboard NOAA-20 (N20), and it jointed on orbit the previous VIIRS instrument operating on the Suomi NPP (SNPP) spacecraft since November 2011. During post-launch testing, the accuracy of VIIRS sensor data record (SDR) geolocation products was evaluated using a system called ground control point matching. The control points are based on 30-m Landsat images as "ground truth," and the matchups employ their cross-correlation with the 375-m VIIRS images in band I1. Initial N20 VIIRS geolocation errors shortly after launch exceeded 2 km and were somewhat larger than those previously observed for SNPP VIIRS. The optimization of processing parameters successfully reduced the geolocation uncertainty to less than 400 m (at nadir, 3-sigma), which is comparable to the current performance for the SNPP VIIRS SDR products, with the majority of the geolocation errors within 200 m. The improvement was achieved by adjusting only the instrument-to-spacecraft rotation angles (the "mounting matrix"). Although the uncertainty evaluation was based on global matchups collected over 12-month periods, the parameter optimization was based on a reduction of the geolocation angular errors by reprocessing VIIRS SDR and re-analyzing the global matchups from 16-day orbit repeat periods. Geolocation of the 750-m day/night band (DNB), which is not co-registered with the 375-m I-bands and the 750-m M-bands, was evaluated and optimized separately, using the correlation between DNB and the I1 band re-projected images. Initial N20 VIIRS DNB geolocation errors were even larger than those observed for the other bands, but they were also successfully reduced by adjusting DNB-specific processing parameters. The initial improvements in the N20 VIIRS geolocation accuracy were achieved in 2018, and the processing parameters were further refined after an optical model correction in 2021.

Keywords: Joint Polar Satellite System; National Oceanic and Atmospheric Administration-20; Visible-Infrared Imaging Radiometer Suite; geolocation

Paper 230029G received Jan. 26, 2023; revised Aug. 14, 2023; accepted Aug. 22, 2023; published Sep. 4, 2023.

*Address all correspondence to Slawomir Blonski, Slawomir. Blonski@noaa.gov

1 Introduction

The second satellite in the Joint Polar Satellite System (JPSS) series, the JPSS-1 spacecraft, was launched in November 2017 to become one of the National Oceanic and Atmospheric Administration (NOAA) weather satellites under the designation of NOAA-20 (N20). It operates on the same orbit as the Suomi National Polar-orbiting Partnership (SNPP) satellite launched in October 2011, but with the separation between the two spacecraft being approximately equal to half of the orbital period. Visible-Infrared Imaging Radiometer Suite (VIIRS) is one of five Earth remote sensing instruments onboard both N20 and SNPP.[1–5] VIIRS sensor data record (SDR) products include radiometric measurements in 22 channels (from the 0.4 to 12.5 μm spectral range) as well as their geolocation, with and without terrain correction, at two spatial resolutions: 750 m [separately for moderate-resolution bands, M1 to M16, and the day/night band (DNB)] and 375 m (imagery bands, I1 to I5). Accurate VIIRS geolocation is essential for many VIIRS data products, such as imagery, polar wind vectors, clouds, aerosol, ocean color, sea surface temperature, and active fires. Moreover, VIIRS observations have the finest spatial resolutions among all instruments onboard the JPSS satellites, and accurate VIIRS geolocation products are critical as a ground reference in evaluating geolocation errors for the other instruments, including Advanced Technology Microwave Sounder (ATMS),[6] Cross-track Infrared Sounder (CrIS),[7] and Ozone Mapping and Profiler Suite (OMPS).[8]

Five VIIRS geolocation datasets are produced in the NOAA operational processing including non-terrain corrected (ellipsoid) geolocation for I-bands (denoted GIMGO) and M-bands (GMODO), terrain corrected geolocation for I-bands (GITCO) and M-bands (GMTCO), and DNB geolocation (GDNBO), although distribution and archiving of the GIMGO and GMODO products may be discontinued in the future. VIIRS I-bands and M-bands are well co-registered band to band, with four (2×2) I-band pixels nested to one M-band pixel. The VIIRS geolocation algorithm first calculates the geolocation of the I-band pixels, and then the M-band geolocation is aggregated from the I-band data, except for the near-nadir M-band pixels for which full geolocation is calculated. The geolocation algorithm for DNB is similar to that of the I-bands, but it is executed separately, and the geolocation data both with and without terrain correction reside in the same product. The evaluated VIIRS SDR products that included the terrain-corrected geolocation were generated by the JPSS interface data processing segment (IDPS) and were accessed through the Government Resources for Algorithm Verification, Independent Test and Evaluation (GRAVITE) and NOAA Center for Satellite Applications and Research (STAR) data portals. These datasets are also available from the NOAA Comprehensive Large Array-data Stewardship System (CLASS) archive.

VIIRS geometric calibration is based on models of the instrument, the Earth, and the spacecraft orbit.[9] The geolocation algorithm uses Earth ellipsoid and geoid/terrain surface information in conjunction with spacecraft ephemeris and attitude data as well as knowledge of the VIIRS instrument and satellite geometry to compute geodetic coordinates (latitude and longitude) and related parameters for each SDR pixel. When terrain correction is not applied, the algorithm intersects each pixel's line of sight with the World Geodetic System 1984 (WGS84) ellipsoid and outputs geodetic latitude and longitude. When the terrain correction is performed, the algorithm determines each pixel's line of sight intersection with the Earth terrain elevation model and outputs terrain corrected geodetic latitude and longitude. Terrain correction adjusts the geolocation for the parallax effect and therefore generates more accurate latitudes and longitudes for off-nadir pixels over elevated surfaces.

JPSS ground system requirements specify that VIIRS geolocation data products shall have a 3-sigma geolocation uncertainty of 400 m at nadir and 1500 m at edge of scan for all bands.[10] It is further defined that, for a suitable ensemble of geolocation measurement and truth data pairs, the 3-sigma geolocation uncertainty is the maximum error value of 99.7% of all error measurements and, in verification, 99.7% of all ensemble error values must be at or less than the requirement value. This means that if 1000 nadir-equivalent geolocation errors are measured, only 3 of them can exceed 400 m. Thus, the estimates of the VIIRS geolocation uncertainty are mostly influenced by the error outliers and require a sufficiently large number of the measurements to minimize effects from single outliers.

Geolocation/pointing accuracy of the N20 VIIRS radiometric measurements was initially evaluated during post-launch testing, and it was subsequently improved by generating updated

parameters for the processing software deployed in the ground system.[11] Although uncertainty of the geolocation products prior to on-orbit calibration was larger than specified in the mission requirements, it was promptly improved after launch by adjusting the SDR processing parameters based on validation as feedback. Although VIIRS pointing knowledge was thoroughly measured during pre-launch testing on both the instrument and spacecraft levels, post-launch optimization of the processing parameters was still required. The improvement in the geolocation accuracy was achieved by optimizing only the instrument-to-spacecraft mounting matrix rotation angles, and changes to the optics model parameters were not needed to reduce the geolocation uncertainty to within the requirements. This approach allowed for timely transition of the VIIRS SDR geolocation products to NOAA operational use within the expected period of three months after the satellite launch. An alternative approach that additionally optimizes the optical model parameters required more time to achieve comparable results for SNPP and N20.[12,13]

2 Methodology

2.1 Geolocation Error Measurements

The nadir-equivalent circular (or radial) errors were calculated from outputs of the control-point matching (CPM) program. The CPM program has been developed previously by NASA to characterize MODIS geolocation errors, and it was later adapted for VIIRS.[12] For VIIRS, the geolocation errors are computed by cross correlation of VIIRS daytime data in band I1 (600 to 680 nm) with spatially aggregated data in the Landsat "red" band (630 to 690 nm). The 30-m ground sample distance of the Landsat data allows for finding the optimal shift of the aggregated Landsat data that provide the maximum correlation to the VIIRS data with the 375-m resolution (at nadir). The evaluation uses 800-by-800 pixel subsets of Landsat data that form ground control point (GCP) "chips." Landsat geolocation data for each chip provide the ground "truth," and VIIRS geolocation data with the best match to the shifted Landsat data are the GCP observations. Outputs of the CPM program include latitude, longitude, and height above the WGS84 ellipsoid for the ground-truth and observed GCPs. Spacecraft position and attitude at the time of the GCP observation are provided as well. VIIRS geolocation errors were measured by calculating the distance on the WGS84 ellipsoid between points with latitude and longitude of the ground-truth and observed GCPs.

Similar analyses of geolocation accuracy based on pre-selected set of GCP chips were previously conducted for MODIS,[12] AVHRR,[14] and MERIS.[15] Significant efforts were also dedicated to increase the number of the chips available for the matchups and to make the chips more consistent with the current ground surface.[16] In a more recent approach, much larger sets of GCPs were dynamically created for selected Earth scenes and applied in the geolocation evaluation for the MERSI-II sensor.[17] In another approach, a large set of GCPs was created from the terrain elevation data along coastlines and was applied for the geostationary imaging sensors from the GEOS and Himawari satellites.[18]

The number of globally distributed GCP chips that were selected for characterization of the N20 VIIRS geolocation errors was 1179. CPM results used in the evaluations of the VIIRS SDR data were produced at STAR with a step of 0.2 pixel-size before the optimization ("on-orbit calibration") of the geolocation processing parameters and 0.05 pixel-size after the optimization. In addition to the geolocation errors, the CPM program also provides a value of image cross-correlation obtained for each matchup. The cross-correlation values measure the quality of the matchups. CPM results generated for the N20 VIIRS SDR both before and after the optimization contained clusters of matchups with high cross-correlation. This enabled the selection of a cross-correlation threshold that allows for using in analysis only the matchups with the highest quality. The threshold of 0.975 was selected for the evaluations of compliance with the geolocation requirements, but that needed accumulation of the GCP matchups over 12-month periods, resulting in about 3000 matchups for each year. Time dependence of the geolocation errors was studied with finer temporal resolution using 16-day periods and the threshold of 0.9, typically providing about 700 matchups for each period.

2.2 Transformations to Angular and Nadir-Equivalent Errors

As described in the VIIRS geolocation ATBD,[9] to produce geolocation data for VIIRS radiometric measurements, several transformations need to be applied to convert detector position on

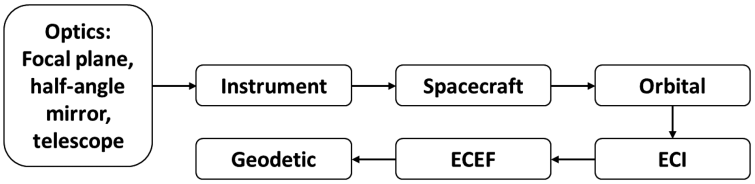

Fig. 1 Coordinate systems used in the VIIRS pointing and geolocation algorithm.

a focal plane to geodetic coordinates of a location observed on the Earth surface (Fig. 1). The first transformation to the instrument coordinate system is based on a model of the VIIRS optics that includes the rotating telescope and the half-angle mirror (HAM) that "de-rotates" the optical image.

The next transformation, from the instrument to spacecraft coordinates, is based on the instrument-to-spacecraft alignment information (the "mounting matrix"). Spacecraft attitude (the roll, pitch, and yaw angles) is used for transformation between spacecraft and orbital coordinates. Transformation between orbital and Earth-centered inertial (ECI) coordinates is derived from the spacecraft position and velocity vectors. ECI coordinates can be transformed into non-inertial Earth-centered Earth-fixed (ECEF) coordinates, and vice versa, using known astronomical parameters. These four transformations can be represented as a series of three-dimensional rotations, as shown in the following equation:

$$u_{\mathrm{ECEF}} = T_{\mathrm{ECEF/ECI}} \cdot T_{\mathrm{ECI/orb}} \cdot T_{\mathrm{orb/sc}} \cdot T_{\mathrm{sc/instr}} \cdot u_{\mathrm{instr}}. \quad (1)$$

Transformation between ECEF and geodetic coordinates is also well defined. Geolocation errors (displacements) in the geodetic coordinates were converted to angular errors in the instrument coordinate system by inversing the above transformations, simplified by orthogonality of the rotation matrices. The nadir-equivalent geolocation errors were calculated by multiplying the angular errors by the distance between the satellite and a sub-satellite point on the Earth's surface (approximated by the WGS84 ellipsoid).

2.3 Minimization of Geolocation Errors

Uncertainty of the N20 VIIRS geolocation products was reduced by minimizing the root-mean-square of the angular errors. The improvement was achieved by adjusting only the instrument-to-spacecraft rotation angles through multiplying the mounting matrix by a corrective rotation matrix. The three correction angles were optimized using the Nelder–Mead method that offers robust performance while requiring only a limited number of goal function evaluations by applying predefined transformations ("reflection," "expansion," "contraction," and "shrink") to the optimized parameters.[19] The optimized mounting matrix is valid for the specific VIIRS optics model that is implemented in IDPS, and when that model was corrected, the matrix had to be re-optimized. The mounting matrix optimizations were based on all global GCP matchups collected over a 16-day JPSS orbit repeat period. Because shortly after launch of the N20 satellite the number of available cloud-free Earth observations was limited, the initial optimization of the mounting matrix was based on reprocessing a small set of VIIRS SDR from North Africa and the Middle East. The suitability of that approach was demonstrated previously.[20] Subsequent mounting matrix optimizations that further reduced the geolocation uncertainty were based on full 16-day datasets from the same area, but even that had to be extended to global matchups to achieve the desired accuracy while limiting the number of needed iterations. Although the geolocation errors are calculated for the terrain-corrected VIIRS SDR products, the mounting matrix optimization based on the angular errors omits the effects from terrain correction. The effects for rough terrain seem to be negligible on the global scale used in the optimization, but several iterations of the optimization followed by reprocessing of the used dataset were done to ensure that it is indeed the case. Reprocessing the VIIRS SDR data with the optimized geolocation parameters was conducted using the Algorithm Development Library (ADL) software that incorporates the computer code deployed in IDPS.

2.4 DNB Adjustments

Although only band I1 is used to maintain VIIRS geolocation accuracy, band-to-band registration between band I1 and the other I-bands as well as the M-bands ensures that those bands have comparable geolocation uncertainty. However, DNB is not co-registered with the other bands. Although the DNB ground sampling distance is nearly constant along the cross-track scan, due to sub-pixel aggregation of detector arrays, it increases away from nadir for the I-bands and the M-bands. Because detector arrays for both the DNB and band I1 are on the same focal plane, DNB geolocation can be tied up with I1. Single, near-nadir point (a west Sahara river mouth) was initially used to achieve agreement between DNB and I1 geolocation by adjusting a processing parameter specific to the positions of the DNB detectors. DNB geolocation was later refined by optimizing that parameter to achieve maximum cross-correlation between a near-nadir subset of a DNB image (512 by 512 pixels) and an I1 image re-projected to the latitude and longitude of the DNB pixels. It is also possible to use cross-correlation for the entire VIIRS granule to align DNB and I1, but it was not applied for N20 because of the modification of the DNB aggregation scheme that was done to avoid the effects of radiometric response nonlinearity.[3]

2.5 Evaluation of Geolocation Uncertainty

Although the uncertainty evaluation is based on global matchups collected over a 12-month period, even with more than 1000 of the GCPs, the applied CPM program collects over that time period only about 3000 GCP matchups that exceed the selected cross-correlation threshold. That seems barely sufficient to estimate the geolocation uncertainty just by counting the errors within the required range. Instead, the Burr Type XII distribution was used to approximate the probability distribution of the geolocation errors,[21] to estimate its parameters, and to predict the 99.7% level of the cumulative distribution that provides the geolocation uncertainty. As the circular errors are never negative, their random distribution is described by Poisson statistics better than by Gaussian statistics, and the Burr distribution provides the best fit to it using two shape parameters and a scale parameter to express a wide range of distribution forms, such as gamma, log-normal, log-logistic, and bell-shaped.

3 Results

3.1 Initial Post-Launch Calibration

For the N20 VIIRS geolocation error evaluation before the optimization (on-orbit calibration) of the processing parameters, nine days without significant disturbances of the satellite orbit were selected: 21, 22, 24, 25, 27, 28 December 2017 and 1, 2, 4 January 2018. Although it was not possible to select for the initial evaluation all 16 days from the full orbit repeat period, Fig. 2 shows that a sufficient number of GCP matchups was collected, even with the applied cross-correlation threshold of 0.9. A cluster of matchups with high cross-correlation can be identified on the graph shown in Fig. 2 (top left). This enables using a cross-correlation threshold to select matchups with the highest quality. When only those matchups are applied in the evaluation, the determined N20 VIIRS geolocation errors prior to the on-orbit calibration are around 2 km, as shown in Fig. 2 (bottom left). Such large geolocation errors can also be seen on VIIRS images when re-projected to geographic coordinates and compared with known geolocation of coastlines and other recognizable objects. Figure 2 also shows that many of these selected GCP matchups are located in North Africa and the Middle East.

To evaluate geolocation errors after the first mounting matrix optimization and deployment of the updated processing parameters in IDPS on January 5, 2018, VIIRS SDR products from 16 consecutive days (January 7 to 22, 2018) without significant orbit disturbances were analyzed. Figure 3 shows the nadir-equivalent geolocation errors determined from the CPM program outputs with and without applying the cross-correlation threshold of 0.9. The errors were clearly reduced by the mounting matrix optimization from about 2 km to typically <200 m.

Figure 4 shows the angular errors, decomposed into the roll, pitch, and yaw directions, before and after the first optimization of the mounting matrix. Despite scatter of the measured points, biases of approximately 400 arcsec in the roll direction and −200 arcsec in the pitch direction can be seen before the optimization. These biases clearly diminished after the optimization.

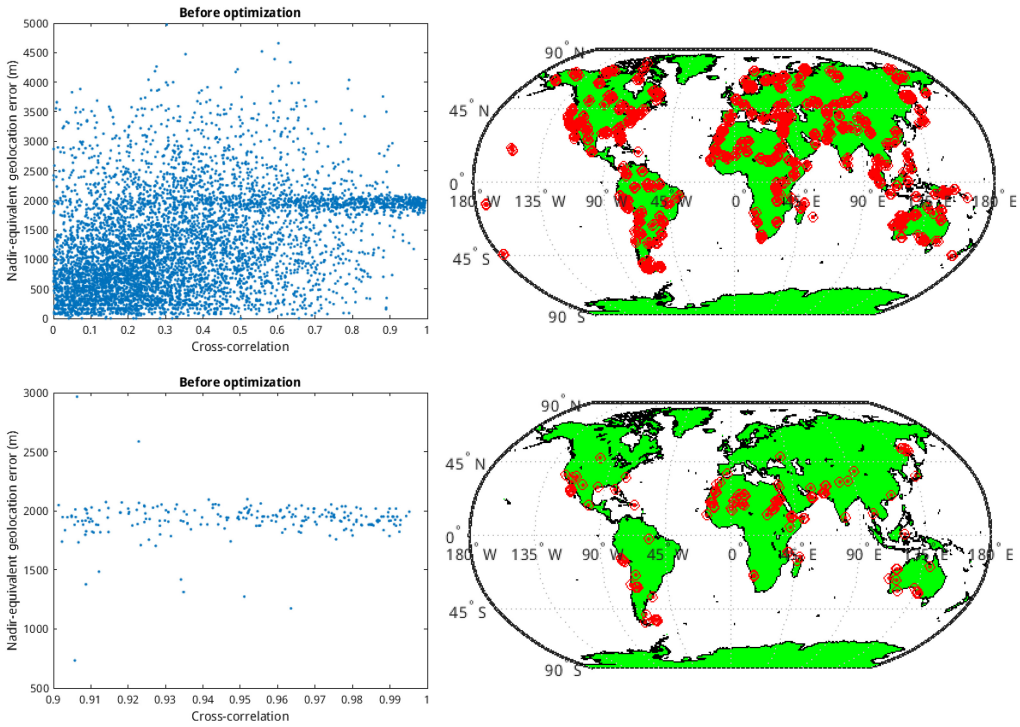

Fig. 2 Nadir-equivalent geolocation errors (left) and global maps of the GCP matchups (right) analyzed with (bottom) and without (top) applying the cross-correlation threshold of 0.9.

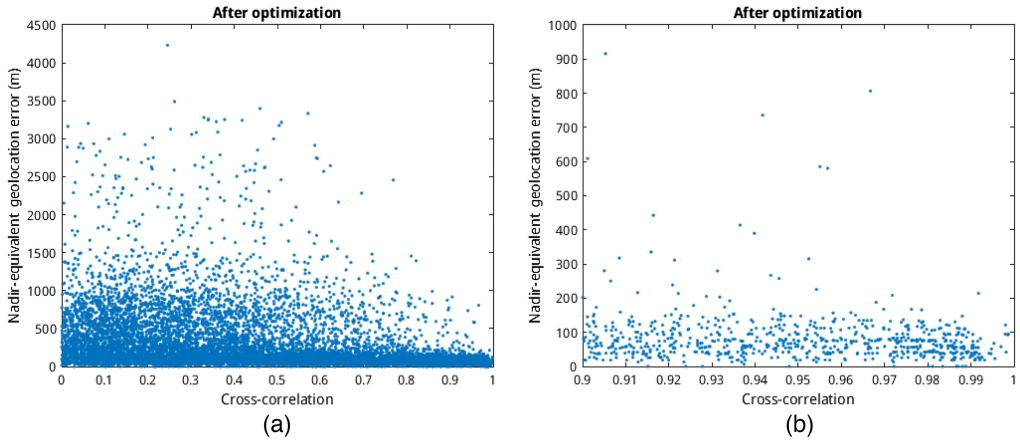

Fig. 3 N20 VIIRS nadir-equivalent geolocation errors after the initial on-orbit calibration analyzed with (b) and without (a) applying the cross-correlation threshold of 0.9.

3.2 Further Geolocation Improvements

Subsequent to the initial post-launch update of the mounting matrix in early January 2018, five updates of the VIIRS geolocation processing parameters were made during the first 5 years of the N20 operations on orbit. The first of these updates was made in February 2018 after a full set of 16-day data became available, allowing for re-optimization of the mounting matrix. The second update was in May 2018 when updated parameters for VIIRS optical model became available and thermal conditions stabilized after the "mid-mission" outgassing conducted in March 2018. The third update (in October 2019) added parameters for seamless switching between two "sides" of the scan controller electronics in case it needs to be done on orbit, but it did not change the existing geolocation calculations. In addition to the correction of the VIIRS optical model,[13] the fourth update (in February 2021) included optical model parameter values derived from the pre-launch measurements conducted for N20 VIIRS by the manufacturer. The updated values

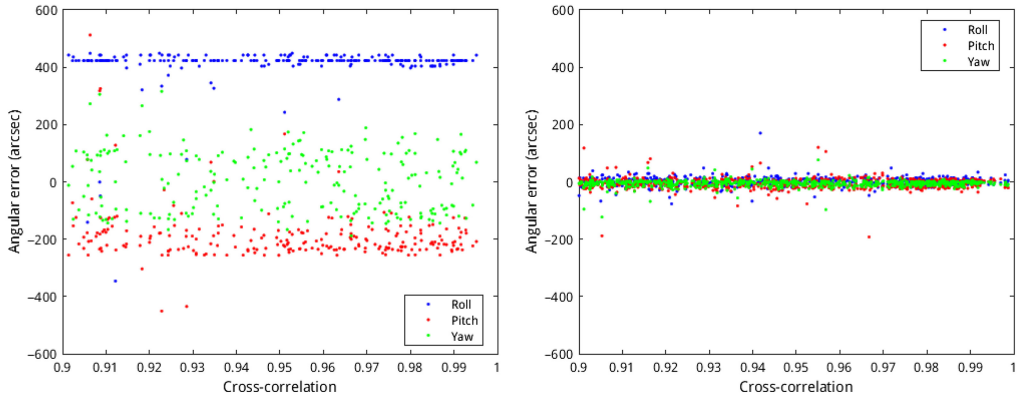

Fig. 4 Roll, pitch, and yaw components of the angular errors before (a) and after (b) the initial on-orbit calibration of the N20 VIIRS geolocation processing parameters.

replaced the SNPP VIIRS ones used previously. The optimization of the mounting matrix for that update was not fully successful, adding small biases to the geolocation errors, and the fifth update (a re-optimized mounting matrix) was deployed in July 2021. The improvement was achieved by analyzing global GCP matchups instead of those located in North Africa and the Middle East only. Values of the parameters from the latter update are listed in Table 1. Although the instrument-to-spacecraft roll/pitch/yaw angles were obtained by the mounting matrix optimization, the HAM alpha/beta/gamma angles, defined in ATBD,[9] are from the measurements acquired during VIIRS pre-launch testing. The table also shows corresponding values obtained at NASA by optimizing all six parameters for processing NASA level 1b products.[13]

In addition to being applied to improve the accuracy of the geolocation products, the angular corrections derived for the 16-day periods were also used to monitor the geolocation errors over timeline of the N20 mission. Figure 5 shows that, following the adjustments of the geolocation processing parameters in 2018, the angular errors display annual oscillations that periodically

Table 1 Major geolocation parameter values for NOAA-20 VIIRS.

	Parameter (arcsec)	NOAA IDPS November 2017	NOAA IDPS January 2018	NOAA IDPS February 2018	NOAA IDPS May 2018
Instrument-to-spacecraft mounting matrix	Roll	1.0	−420.8	−420.9	−412.5
	Pitch	51.1	286.4	296.8	297.5
	Yaw	80.5	93.0	114.3	114.4
HAM angles	Alpha	3.9	3.9	3.9	−4.4
	Beta	9.5	9.5	9.5	9.5
	Gamma	−6.0	−6.0	−6.0	1.0

	Parameter (arcsec)	NOAA IDPS October 2019	NOAA IDPS February 2021	NOAA IDPS July 2021	NASA Land SIPS Collection 2.1[13]
Instrument-to-spacecraft mounting matrix	Roll	−412.5	−359.1	−359.7	−363.6
	Pitch	297.5	290.5	295.0	295.4
	Yaw	114.4	111.5	113.6	112.6
HAM angles	Alpha	−4.4	3.7	3.7	9.2
	Beta	9.5	2.8	2.8	−15.9
	Gamma	1.0	0	0	−2.6

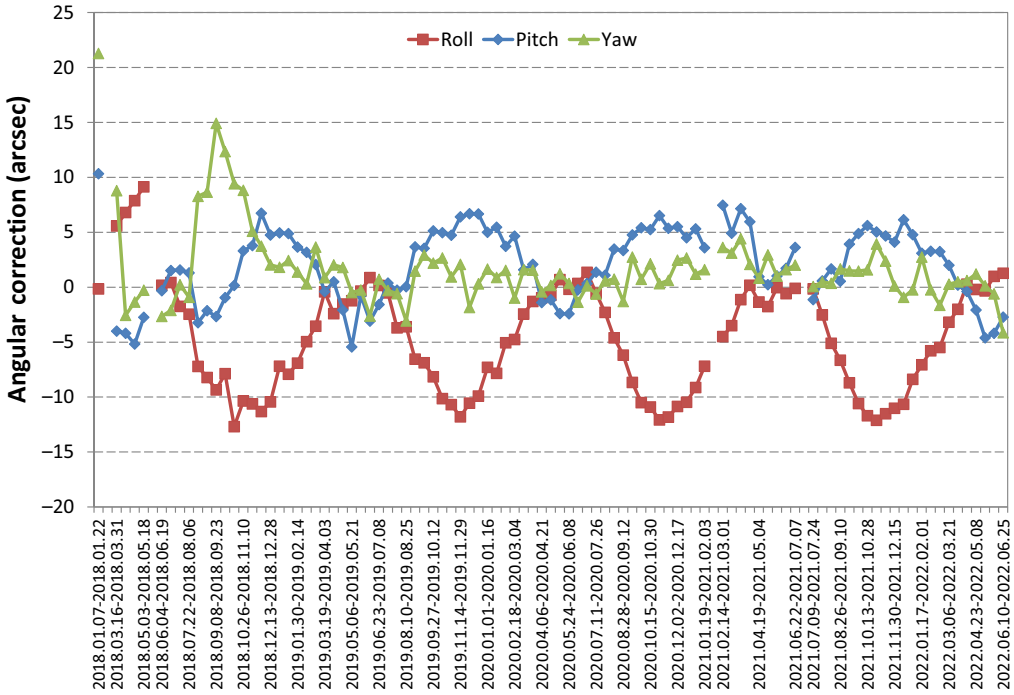

Fig. 5 Time series of the roll, pitch, and yaw components of the angular error corrections for the N20 VIIRS SDR geolocation products. The breaks in the plotted lines indicate updates of the geolocation processing parameters.

increase the geolocation errors by up to about 50 m on the ground. These oscillations are most likely a thermal effect, and a correction was developed based on the day of year. This correction has not been implemented yet in the operational processing due to software engineering concerns. Additionally, an increase of a few arcseconds in the pitch and yaw biases can be seen in Fig. 5 between February and July 2021 because a limited geographic area was initially used in the mounting matrix optimization, as described in the previous paragraph.

3.3 DNB Adjustments

The image cross-correlation technique was used to refine the accuracy of the DNB geolocation after the initial adjustment of the mounting matrix. Figure 6 shows a composite image with the different color layers displaying subsets of a DNB image and a re-projected band I1 image that were used to adjust the DNB "detector position" parameters. The "grid points" for the re-projection are the DNB pixels to which the I1 pixels are re-projected based on the two geolocation datasets, but these points are not on a grid, and linear interpolation combined with a Delaunay triangulation is used to perform the non-gridded re-projection. The subset images are very similar despite DNB having a broader spectral response than I1, and the composite image appears grayscale. The presented image was generated after the parameter adjustment, and there is almost no shift between the DNB and I1 images in the horizontal direction (along scan). That shift is controlled by the DNB detector position parameter for the scan direction. Cross-correlation between the DNB and I1 images also changes accordingly to allow for the determination of the detector position value that provides the maximum cross-correlation, as shown in Fig. 7. The determined optimal parameter value agrees well with that obtained by Lin et al.[13] based on an independent analysis of cross-correlation between VIIRS DNB and Landsat images.

3.4 Geolocation Uncertainty

To evaluate the uncertainty of the VIIRS SDR geolocation products while using a sufficient number of GCP matchups to limit outlier fluctuations, the time span to collect the data was extended from 16 days to 12 months to allow for increasing the cross-correlation threshold from 0.9 to 0.975. That also allows for accounting for the annual oscillations observed in the geolocation errors. Two examples of histograms and distribution functions generated for the

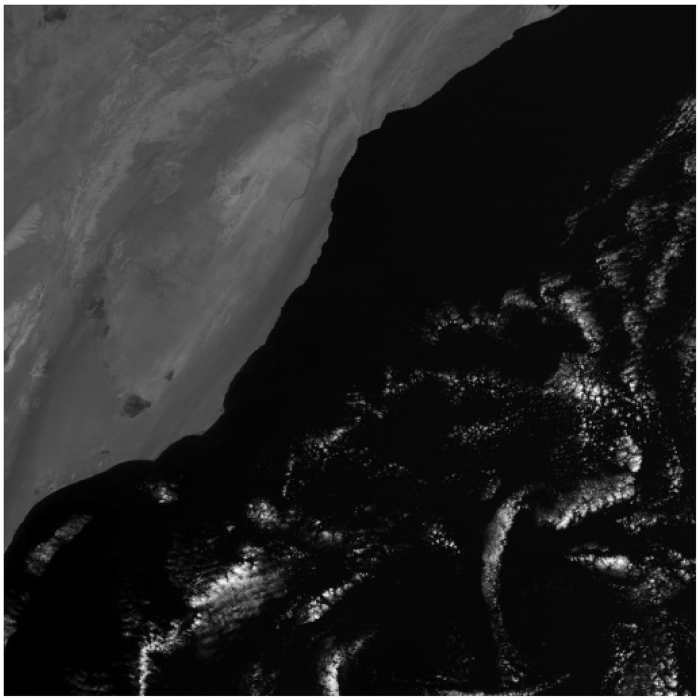

Fig. 6 Composite RGB image showing a DNB image and a re-projected I1 image overlaid in different color layers: such image subsets were used to adjust the N20 VIIRS DNB geolocation processing parameter ("detector position"). Gray regions in the composite image show where the two images have nearly the same intensities, and the magenta and green regions show where the intensities are different (not visible for the optimal detector shift).

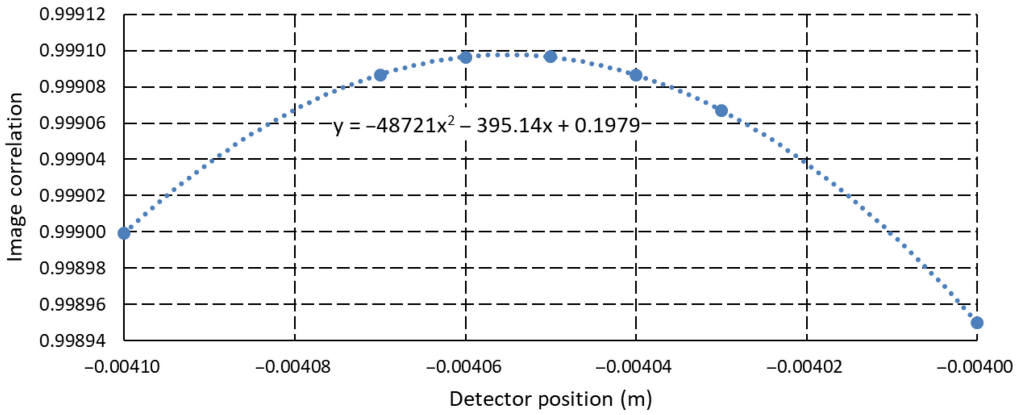

Fig. 7 Cross-correlation between DNB and re-projected I1 images (filled circles) produced with different values of the DNB detector position parameter. The dotted line shows quadratic interpolation of the measured points that supports the determination of the maximum's position.

VIIRS SDR geolocation errors observed over 12-month periods are shown in Fig. 8. The graphs are for the geolocation products generated before and after the VIIRS optical model correction. Estimates of the 3-sigma uncertainty of the geolocation products are also shown on the graphs by the vertical dashed lines. Although the uncertainty appears to be lower before the optical model correction, the distribution of the errors is clearly more complex. Nevertheless, in both cases the estimated uncertainty is well within the product requirements. One may actually notice that most of the VIIRS SDR geolocation errors are in the 200 m range.

Geolocation uncertainty estimates for all 12-month periods since the N20 launch are shown in Fig. 9. Except for the first estimate that includes data from a few days before the initial correction of the mounting matrix in January 2018, the uncertainty remains within the required

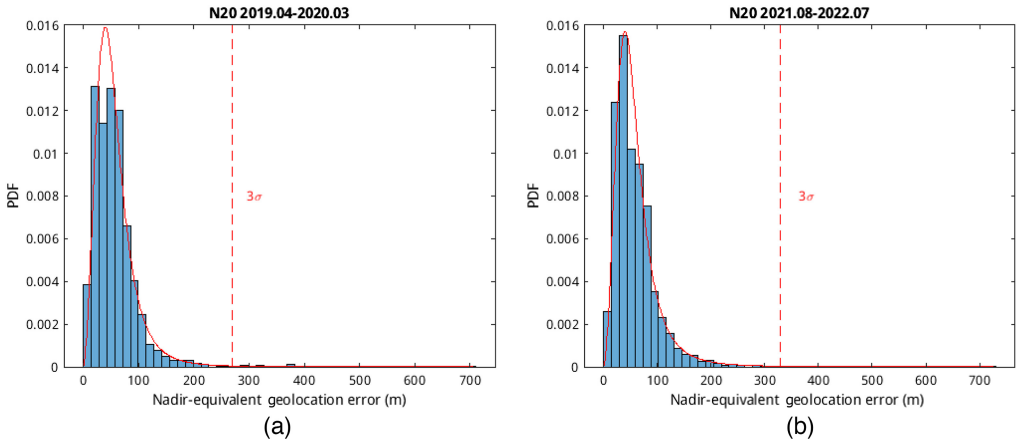

Fig. 8 Two examples of histograms and distribution functions generated for the N20 VIIRS SDR geolocation errors observed over 12-month periods before (a) and after (b) the VIIRS optical model correction in February 2021.

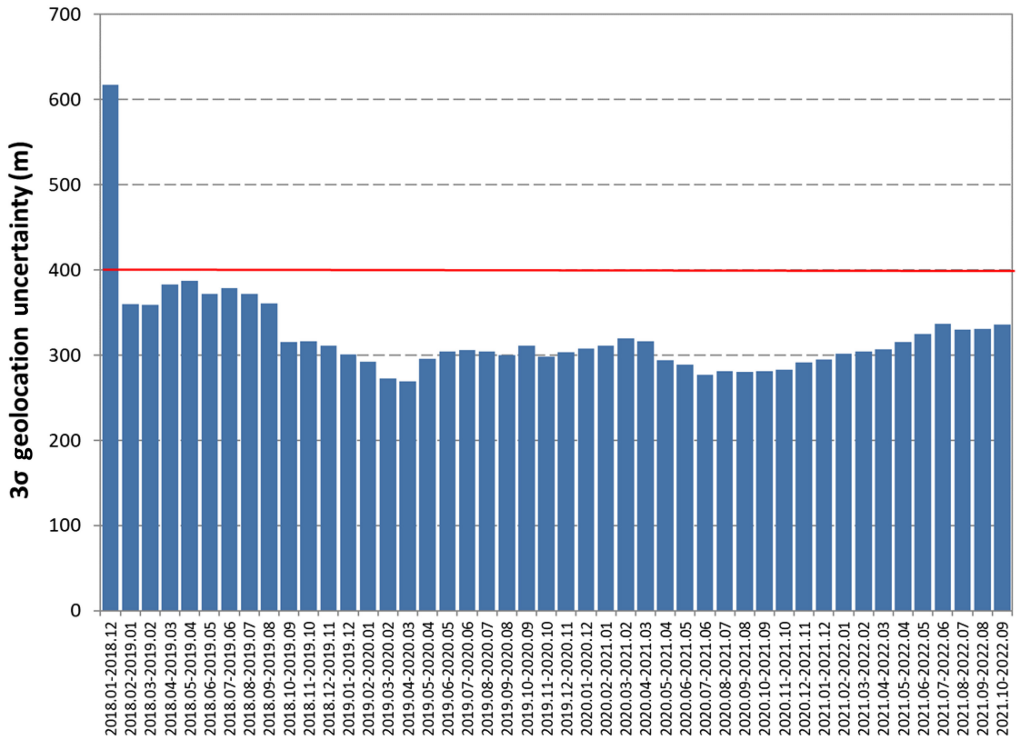

Fig. 9 N20 VIIRS geolocation uncertainty evaluated for the successive 12-month periods since the initial on-orbit calibration. The red line shows the geolocation uncertainty requirement for the N20 mission.

range. There is even a substantial margin from the requirement after the processing parameter optimizations conducted in 2018.

4 Discussion

Although VIIRS pointing knowledge was thoroughly measured during pre-launch testing on both the instrument and spacecraft levels, post-launch optimization of the processing parameters was definitely required. In this study, the improvement in the geolocation accuracy was achieved by only optimizing the mounting matrix rotation angles. Changes to the optics model parameters, such as the HAM angles, were not needed to reduce the geolocation uncertainty not only to

within requirements but also with a substantial margin. Such changes were previously found necessary to improve SNPP VIIRS geolocation accuracy. As the geolocation processing is a series of matrix multiplications, the mounting matrix corrections derived in this work may also include small corrections for the optics model, e.g., the HAM angles, or even for the satellite attitude (pointing) knowledge. Although it is a simplified approach, the presented work demonstrates that it is successful in reducing VIIRS geolocation errors.

The mounting matrix optimization presented in this study was based on minimizing the angular displacements obtained from the CPM analyses. When needed, the optimization was repeated multiple times while reprocessing the geolocation products after each iteration using the updated parameters. Although the minimization of the angular errors omits the terrain correction, the iterations ensured that the terrain effects were included in the updates of the processing parameters.

The presented work has demonstrated that the optimization of the geolocation processing parameters benefits from reprocessing a large number of VIIRS SDR datasets with the global coverage for 16 days or more. Providing computational capabilities for such reprocessing will support the calibration and validation of VIIRS SDR products from future JPSS spacecraft, starting with JPSS-2/NOAA-21 launched in November 2022. Reanalysis of the reprocessed geolocation products with CPM remains an indispensable step in the mounting matrix optimization.

The evaluation of the VIIRS geolocation uncertainty to verify the agreement with the JPSS requirements necessitates collecting thousands of GCP matchups. When using the current CPM software, the time span of the matchups had to be extended to 12 months to collect a sufficient number. An updated CPM software and chip library have been developed,[13] and after it becomes available for the VIIRS SDR evaluations, shorter time spans may be adequate as well.

5 Conclusions

This study presented N20 VIIRS SDR post-launch geolocation accuracy and improvements. The operational VIIRS I/M-bands geolocation products were monitored using the CPM program and for DNB using stable point light sources such as oil platforms. Although uncertainty of the N20 VIIRS SDR geolocation products prior to on-orbit calibration was larger than that specified in the mission requirements, it was promptly improved after launch by the initial post-launch mounting matrix update, with errors reduced from about 2 km to <200 m. Five additional updates of the VIIRS geolocation processing parameters were made during the first 5 years of the N20 operations on orbit. The mounting matrix optimization was based on minimizing the angular displacements obtained from the CPM analyses. Moreover, the image cross-correlation technique was used to refine the accuracy of the DNB geolocation after the initial adjustment of the mounting matrix. Geolocation uncertainty estimates for all 12-month periods since the N20 launch indicate that the uncertainty remains within the required range and with a substantial margin from the requirement after the processing parameter optimizations conducted in 2018.

In this study, the improvement in the N20 geolocation accuracy was achieved by only optimizing the mounting matrix rotation angles. Our results suggest that changes to the optics model parameters were not needed for either meeting the requirements or achieving a substantial margin from them. Future adjustments to the VIIRS geolocation processing algorithm and its parameters may be implemented when found necessary based on the monitoring results, such as the thermal correction to reduce the seasonal oscillations observed for N20 or to incorporate the updated CPM software and chip library.

Code, Data, and Materials Availability

Although access to GRAVITE and NOAA STAR data portals is restricted, public access to JPSS products is provided by NOAA CLASS (http://www.class.noaa.gov/).

Acknowledgments

The presented work was partially funded by the JPSS Program and the NOAA (Grant No. ST1330-17-CQ-0050) as well as the NOAA Cooperative Institute for Satellite Earth System Studies (CISESS) at the University of Maryland/Earth System Science Interdisciplinary Center

(ESSIC) (Grant No. NA19NES4320002). The scientific results and conclusions, as well as any views or opinions expressed herein, are those of the authors and do not necessarily reflect those of NOAA or the Department of Commerce. The authors declare no conflict of interest.

References

1. C. Cao et al., "Early on-orbit performance of the visible infrared imaging radiometer suite onboard the Suomi National Polar-Orbiting Partnership (S-NPP) satellite," *IEEE Trans. Geosci. Remote Sens.* **52**(2), 1142–1156 (2014).
2. C. Cao et al., "Suomi NPP VIIRS sensor data record verification, validation, and long-term performance monitoring," *J. Geophys. Res. Atmos.* **118**(20), 11664–11678 (2013).
3. W. Wang and C. Cao, "NOAA-20 VIIRS DNB aggregation mode change: prelaunch efforts and on-orbit verification/validation results," *IEEE J. Sel. Top. Appl. Earth Obs. Remote Sens.* **12**(7), 2015–2023 (2019).
4. T. Choi et al., "NOAA-20 VIIRS reflective solar band postlaunch calibration updates two years in-orbit," *IEEE Trans. Geosci. Remote Sens.* **58**(11), 7633–7642 (2020).
5. W. Wang and C. Cao, "NOAA-20 and S-NPP VIIRS thermal emissive bands on-orbit calibration algorithm update and long-term performance inter-comparison," *Remote Sens.* **13**(3), 448 (2021).
6. C.-H. Lyu, et al., "JPSS-1 ATMS postlaunch active geolocation analysis," *IEEE Trans. Geosci. Remote Sens.* **59**(11), 9462–9471 (2021).
7. L. Wang, et al., "Improved scheme for Cross-track Infrared Sounder geolocation assessment and optimization," *J. Geophys. Res. Atmos.* **122**(1), 519–536 (2017).
8. L. Wang, et al., "Geolocation assessment and optimization for OMPS Nadir Mapper: methodology" *Remote Sens.* **14**(13), 3040 (2022).
9. "Joint Polar Satellite System (JPSS) VIIRS Geolocation Algorithm Theoretical Basis Document (ATBD)," https://www.star.nesdis.noaa.gov/jpss/Docs.php (accessed October 2022).
10. "Joint Polar Satellite System (JPSS) Ground Segment Data Product Specification (GSegDPS)," https://www.nesdis.noaa.gov/s3/2022-03/474-01543_JPSS-GSegDPS_A.pdf (accessed October 2022).
11. S. Blonski, W. Wang, and C. Cao, "Post-launch evaluation and improvements of NOAA-20 VIIRS geolocation accuracy," *Proc. SPIE* **10785**, 1078518 (2018).
12. R. E. Wolfe et al., "Suomi NPP VIIRS prelaunch and on-orbit geometric calibration and characterization," *J. Geophys. Res. Atmos.* **118**(20), 11508–11521 (2013).
13. G. Lin et al., "Ten years of VIIRS on-orbit geolocation calibration and performance," *Remote Sens.* **14**(17), 4212 (2022).
14. M. Schmidt, E. A. King, and T. R. McVicar, "Assessing the geometric accuracy of AVHRR data processed with a state vector based navigation system," *Can. J. Remote Sens.* **34**(5), 496–508 (2008).
15. P. Bicheron et al., "Geolocation assessment of MERIS GlobCover Orthorectified products," *IEEE Trans. Geosci. Remote Sens.* **49**(8), 2972–2982 (2011).
16. P. Zhang et al., "Ground control points refresh for MODIS and VIIRS geolocation monitoring," *Proc. SPIE* **11829**, 118290Y (2021).
17. H. Pan et al., "Systematic geolocation errors of FengYun-3D MERSI-II," *IEEE Trans. Geosci. Remote Sens.* **60**, 5619711 (2022).
18. W. Wang et al., "An Introduction to the Geostationary-NASA Earth Exchange (GeoNEX) products: 1. Top-of-atmosphere reflectance and brightness temperature," *Remote Sens.* **12**(8), 1267 (2020).
19. J. C. Lagarias et al., "Convergence properties of the Nelder-Mead Simplex method in low dimensions," *SIAM J. Optim.* **9**(1), 112–147 (1998).
20. W. Wang, et al., "Assessment of the NOAA S-NPP VIIRS geolocation reprocessing improvements," *Remote Sens.* **9**(10), 974 (2017).
21. P. R. Tadikamalla, "A look at the Burr and related distributions," *Int. Stat. Rev.* **48**(3), 337–344 (1980).

Slawomir Blonski received his master's degree in applied physics from the Gdansk University of Technology, Gdansk, Poland, in 1985 and his PhD in physics from the University of North Texas, Denton, Texas, United States, in 1991. His earlier works included modeling of Fourier-transform infrared spectrometers, spatial resolution determination for the initial commercial remote sensing satellites, and simulations of lower-resolution Earth observations from actual data acquired with higher spatial and spectral resolutions. He currently works on the calibration and validation of the Visible Infrared Imaging Radiometer Suite instruments and their remote sensing products.

Wenhui Wang received her BS and MS degrees in computer science from Xi'an Jiaotong University, Xi'an, China, in 1991 and 1994, respectively and her PhD in geography specializing in remote sensing from the University of Maryland, College Park, Maryland, United States,

in 2008. From 1994 to 2001, she was a senior software engineer with the Institute of Computing Technology, Chinese Academy of Sciences, Beijing, China. From 2008 to 2013, she was a support scientist with I. M. Systems Group, Inc., Rockville, Maryland, United States. From 2013 to 2018, she was a senior scientist with Earth Resources Technology, Inc., Laurel, Maryland, United States. From 2018 to 2019, she was a senior scientist with Global Science and Technology, Inc., Greenbelt, Maryland, United States. She is currently a visiting associate research scientist with the Cooperative Institute for Satellite Earth System Studies, University of Maryland. Her research interests include satellite instrument calibration and validation, climate data records, surface radiation budget, and geo-visualization.

Khalil Ahmad received his MS degree and PhD in electrical engineering, with an emphasis on satellite remote sensing, from the University of Central Florida, Orlando, Florida, United States, in 2004 and 2007, respectively. He was involved in retrieval algorithm development and calibration/validation of microwave radiometer and scatterometer instruments. He is currently a senior scientist with Global Science and Technology Inc., Greenbelt, Maryland, supporting the calibration and validation activities of the Visible Infrared Imaging Radiometer Suite sensors onboard current operational and future JPSS satellite missions. His principal areas of interest include satellite remote sensing, algorithm development, and the radiometric and geometric calibration/validation of spaceborne microwave and optical sensors.

Changyong Cao is a supervisory physical scientist at the NOAA Center for Satellite Applications and Research. He specializes in the calibration of radiometers on board NOAA's Operational Environmental Satellites and currently leads the VIIRS sensor science team. He was the recipient of three gold and one silver medals honored by the U.S. Department of Commerce for his scientific and professional achievements. He received his PhD in geography specializing in remote sensing and geographic information systems from Louisiana State University in 1992.